Physicochem. Probl. Miner. Process., 54(3), 2018, 803-813

http://www.journalssystem.com/ppmp

Physicochemical Problems of Mineral Processing

ISSN 1643-1049

Received August 11, 2017; reviewed; accepted January 27, 2018

Selective flotation of siderite and quartz from a carbonate-containing refractory iron ore using a novel amino-acid-based collector

Xiaotian Gu[1], Yimin Zhu [1,2], Yanjun Li [1,3], Yuexin Han [1,3]

[1] College of Resource and Civil Engineering, Northeastern University, Shenyang, China

[2] 2011 Collaborative Innovation Centre of Steel Technology, Northeastern University, Shenyang, China

[3] Liaoning Technology and Engineering Laboratory of Effective Exploitation of Refractory Iron Ores, Shenyang, China

Corresponding author: zhuyimin@mail.neu.edu.cn (Yimin Zhu)

Abstract: A novel and highly-efficient amino-acid-based collector, α-ethylenediamine lauric acid (α-EDA-LA), was studied to selectively beneficiate carbonate-containing refractory hematite ores. Single mineral and synthetic mixture flotation tests were carried out to investigate its floating performance. Zeta potential, fourier transform infrared spectroscopy (FTIR) and Density Functional Theory-based molecular simulation were used to identify the adsorption mechanism. The flotation results showed that quartz could be collected effectively at pH 11.0-12.0 in the reverse flotation. For siderite, the recovery peaked at 83.4% at pH 8.0, where siderite presented different floatability from magnetite and hematite. Exploiting such difference, the separation of siderite could be achieved. Zeta-potential measurements showed that α-EDA-LA adsorption on the surfaces of siderite and quartz decreased the corresponding zeta potentials at pH of 8.0-10.0 and 8.0-12.0, respectively. This means the adsorption overcome the electrostatic repulsion between α-EDA-LA and the mineral surfaces. The molecular simulation indicated that no chemisorption took place between α-EDA-LA and quartz. FTIR analysis suggested that α-EDA-LA was adsorbed on quartz via hydrogen bonding. The adsorption of α-EDA-LA on siderite surface was dominated by chemisorption, while further enhanced by hydrogen bonding. This study filled the gap in the research on siderite flotation reagents and its adsorption mechanism.

Keywords: refractory iron ores, hematite, siderite, quartz, flotation, molecular simulation

1. Introduction

Carbonate-containing refractory iron ores refer to the hematite or magnetite ores containing impurities of carbonate minerals such as siderite. By a preliminary estimation, the total reserve of carbonate-containing refractory iron ores in China is more than 5 Pg (Song et al. 2015). Donganshan ore from the northeast of China is typical of such type, which features multiple varieties of minerals, complex microstructure and fine grain sizes. Up until now, there are in total over 20 Tg of carbonate-containing refractory iron ores at Donganshan, which have been categorized as unexploitable resources by the conventional beneficiation technique. The predominant carbonate composition presented in Donganshan ore is siderite. It was found that the presence of siderite considerably deteriorated the flotation. For Donganshan iron ore in particular, siderite content higher than 2.7% will be critical (Zhang et al., 2008).

For the carbonate-containing refractory iron ores, Yin et al. (2010) have come up with a two-step flotation process, which is first to separate siderite from the ore to eliminate its negative effect on flotation and followed by a reverse flotation of gangue minerals typically quartz. This process has been successfully adopted in practice since 2010, giving good production indices. This innovation has effectively reduced the negative effect of siderite imposed on the beneficiation, as well as recovered the siderite resources which have otherwise been considered unexploitable. There has been estimation indicating that around 40% of the potential iron resources in the world are siderite (Tian and Sun, 2010).

http://dx.doi.org/10.5277/ppmp1877

China has large proven reserves of siderite, but most of them are found associated with hematite and magnetite. Single siderite ores are scarce (Tian and Sun, 2010). The fact has undoubtedly bestowed great significance upon the effective utilization of carbonate-containing refractory iron ores. Accordingly, it is of vital importance to develop a powerful flotation reagent aiming for better separation indices. The current widely-used collectors for siderite include cationic collectors, such as lauryl amine, as well as anionic collectors like sodium oleate. However, the publication on novel siderite collectors with better collecting performance is very limited globally. The research on collecting mechanisms between collectors and siderite is even more deficient (Li et al., 2017).

In this research, a novel and highly efficient amino-acid-based collector, α-ethylenediamine lauric acid (α-EDA-LA), has been studied. Single mineral and synthetic mixture flotation tests were carried out to investigate its flotation performance. Zeta-potential measurement, FTIR spectroscopy analysis and density functional theory (DFT)-based molecular simulation were employed to study the adsorption mechanisms. In the two-step flotation process, α-EDA-LA firstly separates siderite from hematite, magnetite and quartz. During the following reverse flotation, α-EDA-LA collects quartz, leaving hematite and magnetite in tailings. This means α-EDA-LA as the collector only interacts with quartz and siderite, but not hematite or magnetite. Therefore, the study focused on the adsorption mechanisms of α-EDA-LA with quartz and siderite.

2. Material and methods

2.1 Mineral sample preparation

The ores of hematite, magnetite, siderite and quartz were purchased and processed to obtain single minerals. The chemical analyses in Table 1 indicate that the purities of the prepared single minerals are closed to the corresponding pure minerals, and therefore meet the requirement for the flotation tests.

Table 1. Chemical analyses of single mineral samples

Content (%)	TFe	$FeCO_3$	FeO	Fe_2O_3	SiO_2	Al_2O_3	MgO	CaO	K_2O	Na_2O
Hematite	68.06	-	0.1100	97.0418	2.4340	0.1253	0.1215	0.0673	-	-
Quartz	-	-	-	0.0642	99.3873	0.4563	-	0.0333	0.0392	0.0418
Siderite	47.01	95.0400	-	-	4.1700	1.2045	3.1201	3.5200	-	-
Magnetite	69.89	-	28.5100	-	0.9387	0.1285	0.0851	0.0500	-	-

The synthetic mixture M1 was prepared by mixing pure magnetite, hematite and quartz in a ratio of 1:2:2, based on their relative mass fractions in Donganshan mixed concentrate of magnetic separation. The synthetic mixture sample M2 was prepared by mixing 5 g M1 with 0.4 g pure siderite, giving a siderite content of 7.41%.

2.2 Reagents

α-EDA-LA and 0.1 mol/dm^3 of HCl / NaOH solutions were used as the collector and pH adjuster, respectively. α-EDA-LA was developed and synthesized by Zhu et al. (2014) at Northeastern University. Its molecular formula is $C_{14}H_{30}N_2O_2$, with the chemical structure shown in Fig. 1.

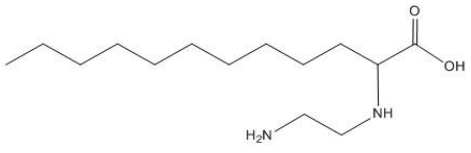

Fig. 1. Schematic diagram: molecular structure of α-EDA-LA

2.3 Single mineral and synthetic mixture flotation tests

Flotation tests were conducted for individual single minerals as well as the synthetic mixtures. A XFG-type flotation machine was used (Gao et al, 2016a, b; Tian et al, 2017; Li and Gao, 2017). To prepare the pulp, the sample of single mineral (2.0g) or synthetic mixture (5.0g) was fed and mixed with certain amount of distilled water. The pulp was stirred for 2 minutes. The pH adjuster and α-EDA-LA were

added successively and stirred for 2 minutes after each reagent addition. The flotation was allowed to proceed for 2 minutes. The foam products and the tailings were collected, dried and weighed. All the tests were done in triplicate to ensure the accuracy. Average was taken and presented on the graphs.

2.4 Zeta-potential measurements

British Malvin Nano-ZS90 model potentiometer was used for the zeta-potential measurements. The prepared single mineral samples were ground further to -20 μm in an agate mortar. 20 mg of the sample was added into 50 cm^3 distilled water and agitated for 15 minutes. The zeta potential was measured in water as well as in the presence of α-EDA-LA. In the cases with the presence of α-EDA-LA, 1 cm^3 α-EDA-LA (10 g/dm^3) was added into the slurry and stirred for 10 minutes. To take the measurements, a representative slurry sample was transferred into the electrophoresis pool by a syringe. The measurements were done in triplicate to ensure the accuracy. Average was taken and presented on the graphs.

2.5 Fourier Transform Infrared Spectroscopy (FTIR) analysis

FTIR spectra were obtained on a 740-FTIR Fourier transformation infrared spectrometer. The spectra were collected in the range of 4000–400 cm^{-1} with 4 cm^{-1} resolution. The single mineral samples were further ground to -20 μm in an agate mortar. To prepare the pulp, 1 g of the sample was mixed with 50 cm^3 distilled water. 1 cm^3 α-EDA-LA (10 g/dm^3) was then added into the pulp. The pulp-collector mixture was agitated for 2 hours, followed by complete sedimentation. The sediment was filtered, washed with distilled water three times and dried at 40°C for 24 hours. The dried cake was mixed with potassium bromide, ground for 15 minutes and then pressed to pelletized discs for FTIR scans.

2.6 DFT-based molecular simulation

Molecular simulation was performed in Material Studio (MS) version 8.0. The geometry of bulk quartz and siderite was optimised as per Zhu et al. (2016) and Li et al. (2017), respectively. Zhu et al. (2016) and Li et al. (2017) reported that quartz (101) surface and siderite (101) surface are the dominant cleavage for the two minerals upon crushing or grinding. Therefore, (101) surfaces of quartz and siderite were chosen for the adsorption mechanism study. The slab surface of quartz was optimised with a slab depth of 22.57Å, vacuum thickness of 10Å, cutoff energy of 460 eV and Monkhorst–Pack mesh of 3x3x4 (Zhu et al., 2016). The supercell was established with 2x2x1 unit cells. For siderite, the slab surface was optimised with 4 layers, a vacuum thickness of 15Å (Li et al., 2017), cutoff energy of 300eV and Monkhorst–Pack mesh of 1x4x1. The siderite supercell was constructed with 2x2x1 unit cells. The structure of α-EDA-LA was optimised in a 20x20x20Å cubic cell with the Brillouin zone restricted to the gamma point. The adsorption of α-EDA-LA on (101) surfaces of quartz and siderite were then simulated.

3. Results

3.1. Single mineral flotation tests

Single mineral flotation tests were carried out to investigate the pH effect on the floatability of hematite, magnetite, siderite and quartz, respectively. The tests were conducted under the conditions of 200 mg/dm^3 α-EDA-LA and 18°C of flotation temperature. The pulp pH was varied within the range from 6 to 12. As per Fig. 2, α-EDA-LA presented excellent collecting ability for quartz, with recovery over 90% throughout the whole tested range of pH. For hematite, the recovery decreased dramatically from 83.4% to 14.2% with the increasing pH. For magnetite, the recovery varied between 59.4% and 83.3%. The floatability of quartz is higher than those of magnetite and hematite at pH 11.0-12.0, which enables the separation of quartz. In the pH region between 8.0 and 10.0, the recovery of siderite stayed above 70%. It peaked at 83.4% when pH was 8.0, where siderite presented different floatability from magnetite and hematite. Exploiting such difference at pH 8.0 and facilitated by depressants, the separation of siderite from hematite and magnetite could be achieved.

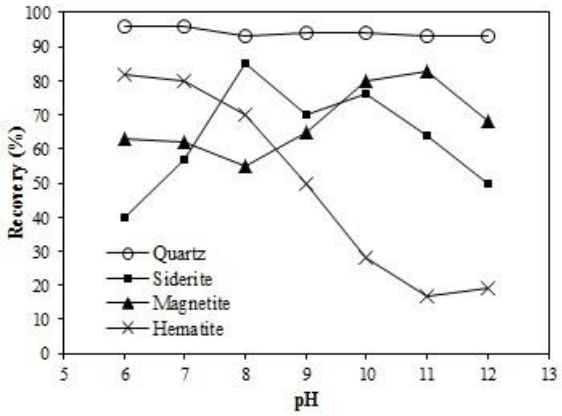

Fig. 2 Relationships between pH and the recovery of single minerals of quartz, magnetite, hematite and siderite (200 mg/dm³ α-EDA-LA, T=18°C)

3.2. Flotation tests on the synthetic mixture sample

3.2.1 Reverse flotation of quartz from synthetic mixture sample M1

Flotation test was carried out for the synthetic magnetite-hematite-quartz mixture M1 to verify the collecting ability of α-EDA-LA for quartz at pH 11.0. The test was conducted with 200 mg/dm³ α-EDA-LA and 20 mg/dm³ carboxyl methyl starch (CMS) as depressant. As in Table 2, the initial Fe grade was 40.86% in the feed. After the reverse flotation, the iron contents were concentrated in the trough product to the grade of 61.53% with Fe recovery of 64.58%. Accordingly, the recovery of quartz in the foam product is 89.65%. These test results prove that α-EDA-LA has better collecting ability for quartz, thus enables the separation of quartz from hematite and magnetite in the reverse flotation process.

Table 2. Results of the reverse flotation test for synthetic mixture M1

Product Name	Yield %	Fe grade %	Fe recovery %	SiO_2 recovery %
Foam product	57.11	25.34	35.42	89.65
Trough product	42.89	61.53	64.58	10.35
Feed	100.00	40.86	100.00	100.00

3.2.2 Direct flotation of siderite for synthetic mixture sample M2

The test was performed under the conditions of 200 mg/dm³ α-EDA-LA, pH 8.0 and 20 mg/dm³ CMS. The test results in Table 3 state that excellent production indices have been achieved with 21.53% siderite content in the concentrate and as low as 4.49% in the trough product. The test results verify the great floating performance of α-EDA-LA for siderite. Hence the amount of siderite left in the trough product would be decreased, which reduces the negative effect of siderite imposed on the following reverse flotation of quartz from other iron-bearing minerals.

Table 3. Results of the flotation test for magnetite-hematite-quartz-siderite synthetic mixture

Product Name	Yield %	Fe grade %	Fe Recovery %	$FeCO_3$ Content %	$FeCO_3$ Recovery %
Foam product	17.13	39.26	16.29	21.53	49.77
Trough product	82.87	41.71	83.71	4.49	50.23
Feed	100.00	41.29	100.00	7.41	100.00

3.3 Zeta potentials of quartz and siderite as a function of pH

Fig. 3 depicts the zeta potential of quartz in water (a) and in the presence of α-EDA-LA (b) as a function of pH. As shown in Fig. 3(a), the potential zero charge (PZC) of quartz is about 2.8, which accords with literature (Vidyadhar and Rao, 2007; Vieira and Peres, 2007). The zeta potential of quartz in water ranged from 5mV to -28mV with the increasing pH from 2.0 to 12.0. Fig. 4 illustrates the zeta potential

of siderite in water (a) and in the presence of α-EDA-LA (b) as a function of pH. As shown in Fig. 4 (a), the PZC of siderite is about 6.2, which agrees with literature (Yang et al., 2010). The zeta potential of siderite in water decreased from 18mV to -19mV with the increasing pH from 4.0 to 12.0.

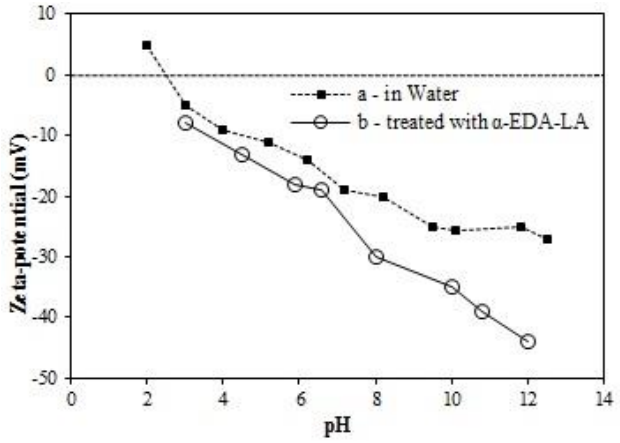

Fig. 3 Relationship between pH and zeta potential of quartz in water (a) and in the presence of α-EDA-LA (b)

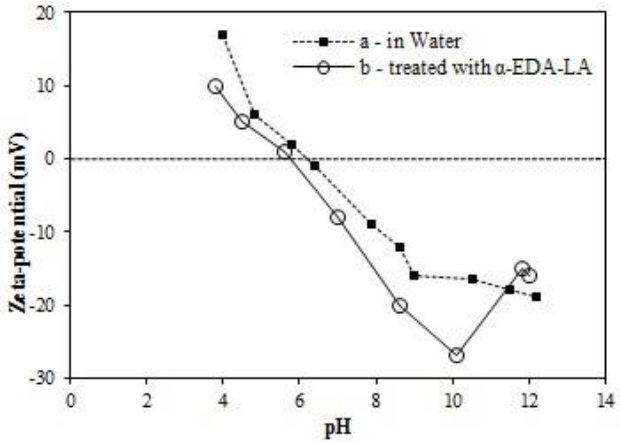

Fig. 4 Relationship between pH and zeta potential of siderite in water (a) and in the presence of α-EDA-LA (b)

3.4 FTIR spectroscopy analyses of quartz and siderite

The FTIR spectra of α-EDA-LA, pure quartz and the quartz treated with α-EDA-LA were recorded in Fig. 5 (a), Fig. 5 (b) and Fig. 5 (c), respectively, at pH of 11.5 and conditioning temperature of 18ºC. The FTIR spectra of α-EDA-LA, pure siderite and the siderite treated with α-EDA-LA were recorded in Fig. 6 (a), Fig. 6 (b) and Fig. 6 (c), respectively, at pH of 8.0 and 18ºC.

The α-EDA-LA molecule contains carboxyl group, primary and secondary amines as shown in Fig. 1. In Fig. 5 (a) and Fig. 6 (a), the intense and broad absorption band at 3440.09 cm^{-1} was composed of the symmetric and asymmetric stretching vibrations of $–NH_2$ and –NH– (Weng and Xu, 2016; Vidyadhar and Rao, 2007). The symmetric and asymmetric stretching vibrations of $–CH_3$ and $–CH_2–$ were defined by the peaks at 2925.81 cm^{-1} and 2842.86 cm^{-1} (Vidyadhar and Rao, 2007). The peak observed at 1706.45 cm^{-1} marked the presence of C=O (Seo et al., 2017). The superposition of the bending vibration of $–NH_2$ and the asymmetric stretching vibration of $–COO^-$ resulted in the 1635.94 cm^{-1} peak (Seo et al., 2017). The band centred at 1403.69 cm^{-1} was attributed to the symmetric stretching vibrations of $–COO^-$ and the in-plane bending vibration of C-O-H. The absorption peaks at 1266.82 cm^{-1} and 1076.04 cm^{-1} corresponded to the stretching vibrations of C-OH and C-N, respectively (Seo et al., 2017; Weng and Xu, 2016). The vibration of $–COO^-$ at 470.51 cm^{-1}. Moreover, broad diffuse bands were observed between 3200 cm^{-1} and 2400 cm^{-1}, which were assigned to the stretching vibration of –OH in the carboxyl group (Weng and Xu, 2016). The hydroxyl groups in carboxylic acids form hydrogen bonds both inter- and

intra-molecularly (Vidyadhar et al., 2003). As a result, carboxylic acids exist as dimmers, which accounts for the diffuse bands induced by vibration modes of –OH.

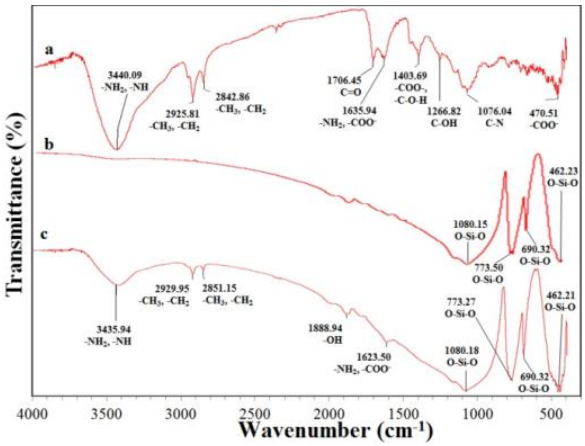

Fig. 5. FTIR spectra of (a) α-EDA-LA (b) quartz (c) α-EDA-LA – quartz at pH=11.5, 18℃

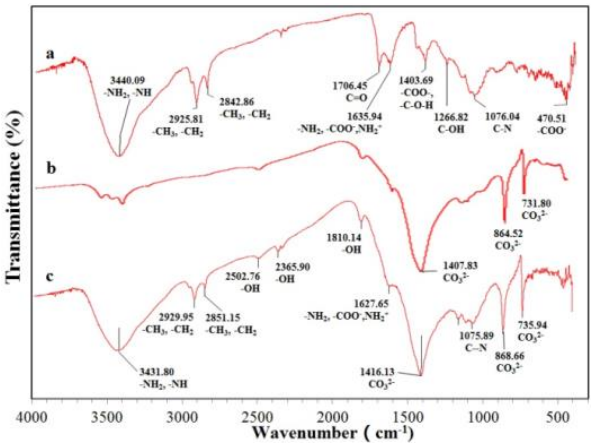

Fig. 6. FTIR spectra of (a) α-EDA-LA (b) siderite(c) α-EDA-LA – siderite at pH of 8.0, 18ºC

3.5 Molecular simulation model validation

With the setting parameters in the models, the unit cell lattice parameters of optimised quartz and siderite agree well with the previous literature (Levien et al., 1980; Graf, 1961) as compared in Table 4. The consistencies prove the validity of the constructed models.

Table 4. Comparison of simulated lattice parameters of quartz and siderite with reference

Parameters	Quartz			Siderite		
	Simulated	Reference	Difference (%)	Simulated	Reference	Difference (%)
a (Å)	4.910	4.916	-0.12%	4.692	4.694	-0.043%
b (Å)	4.910	4.916	-0.12%	4.692	4.694	-0.043%
c (Å)	5.402	5.405	-0.056%	15.38	15.43	-0.32%

4. Discussion

4.1 Collecting mechanism between α-EDA-LA and quartz

4.1.1 Zeta potential of quartz as a function of pH

By comparing Fig. 3 (a) and Fig. 3 (b), it can be seen clearly that the zeta potential of quartz have been significantly reduced in the presence of α-EDA-LA within the pH range from 8.0 to 12.0. In such pH range, α-EDA-LA carries negative charges due to the carboxyl group, which exists in the form of -COO-

under alkali condition. As in Fig. 3 (a), the negative zeta potential of quartz indicates that the quartz surface is also negatively charged at pH of 8.0-12.0. The adsorption of α-EDA-LA on the negatively charged quartz surfaces led to reductions in the zeta potential of quartz. This demonstrates that the adsorption in between was strong enough to overcome the electrostatic repulsion between α-EDA-LA and quartz surface. The strong interaction enables the excellent collecting ability of α-EDA-LA for quartz.

4.1.2 FTIR spectroscopy analysis of quartz

In Fig. 5 (c), the wavenumber region between 1100 cm^{-1} and 400 cm^{-1} contained the infrared spectral features of quartz. The asymmetrical stretching vibration of O-Si-O led to a broad and intense band centred at 1080.18 cm^{-1}. Peaks at 773.27 cm^{-1} and 462.21 cm^{-1} were assigned to the symmetrical stretching vibration of Si-O-Si. The absorption peak at 690.32 cm^{-1} corresponded to the symmetrical bending vibration of Si-O (Mohammadnejad et al., 2013; Chaikina and Kryukova, 2004). The observation of these peaks agrees with the FTIR results exhibited by Sahoo et al. (2016). The infrared spectral features of α-EDA-LA were manifested in the region between 4000 cm^{-1} and 1100 cm^{-1} in Fig. 5 (c). The peaks at 2929.95 cm^{-1} and 2842.86 cm^{-1} confirmed the adsorption of α-EDA-LA on the surface of quartz, as these peaks were due to the stretching vibrations of $–CH_3$ and $–CH_2–$ in α-EDA-LA. Hydrogen bond formation between α-EDA-LA and quartz surface was evident from the peak shifts found by the comparison of Fig. 5 (a) and Fig. 5 (c). FTIR spectroscopy is the most promising experimental technique for hydrogen bonding detection (Muller-Dethlefs and Hobza, 2000). The peak originated from the vibration modes of different functional groups would be affected upon hydrogen bond formation (Ahmed and Jhung, 2017). Thus, the shift of corresponding peaks has been considered an important indicator of hydrogen bonding. The band centred at 3440.09 cm^{-1} in Fig. 5 (a) experienced a 4.15 cm^{-1} shift to 3435.94 cm^{-1} in Fig. 5 (c). The band shift towards lower wavenumber means hydrogen bonds were formed between the nitrogen atoms in amine groups and the electron-deficient hydrogen atoms in the silicanol group exposed on the quartz surface (Mohammadnejad et al., 2013; Vidyadhar et al., 2002; Chernyshova et al., 2000). Similarly, the 12.44 cm^{-1} shift from 1635.94cm^{-1} in Fig. 5 (a) to 1623.50 cm^{-1} in Fig. 5 (c) corroborated the hydrogen bonding between the quartz surface and α-EDA-LA. The oxygen atoms in $–COO^-$ and the nitrogen atoms in the amine groups bonded to the electron-deficient hydrogen atoms in the silicanol group on the quartz surface. The FTIR results suggest that α-EDA-LA was adsorbed on quartz surface via hydrogen bonding, as illustrated in Fig. 7.

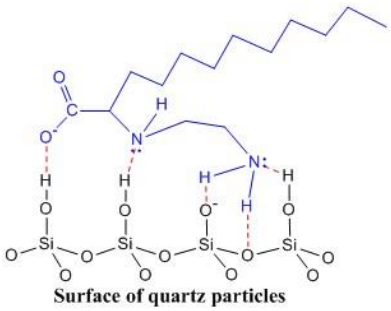

Fig. 7. Schematic diagram: adsorption mechanism of α-EDA-LA on quartz surface (Blue: α-EDA-LA molecule; Black: quartz surface; Red dashed lines: hydrogen bonds; Solid lines: chemical bonds)

4.1.3 Adsorption simulation between a-EDA-LA and quartz

On the hydroxylated (101) quartz surface, the interaction energy of α-EDA-LA is calculated to be -51.02 kJ/mol. The negative value indicates that the adsorption could happen spontaneously. After adsorption, as shown in Table 6, the length of N-H bond within α-EDA-LA increased from 1.031 Å to 1.038 Å, while the distance between $-O^-$ exposed on quartz surface and H atom in amine groups decreased from 3.080 Å to 1.493 Å. This means during interaction the electron-deficient hydrogen atom in amine groups were attracted towards the electron-abundant quartz surface. Similarly, the length of O-H bond exposed on the hydroxylated quartz surface was stretched from 0.986 Å to 1.044 Å due to the attraction force imposed by O^- in carboxyl group and N in the amine groups of α-EDA-LA. The stretched N-H bond

within α-EDA-LA and O-H bond on quartz surface have populations of 0.35 and 0.48, respectively. The positive populations reveal that these chemical bonds were still bonded upon stretching. This proves that the interaction between α-EDA-LA and quartz was not via chemisorption, but resulted from the electronic attraction. This electronic attraction could be due to the hydrogen bonding, which is formed via electron shift between the donor and the acceptor (Schran et al., 2017). As illustrated by Table 5, the populations of 2p orbitals of O and N in α-EDA-LA decreased. On the other hand, the population of H atom on the hydroxylated quartz surface increased from 0.46 to 0.54. The Mulliken population analysis elucidates that the electrons shifted between O, N and H, leading to hydrogen bond formation.

Table 5. Mulliken population analysis of adsorption between α-EDA-LA and quartz surface

Key Atom	Location	Before/after adsorption	s	p	d	Total
O	C-O in α-EDA-LA	before	1.83	4.90	-	6.73
		after	1.84	4.62	-	6.46
O	C=O in α-EDA-LA	before	1.84	4.91	-	6.75
		after	1.83	4.66	-	6.50
N	in α-EDA-LA	before	1.55	4.06	-	5.61
		after	1.53	3.83	-	5.36
H	on hydroxylated quartz surface	before	0.46	-	-	0.46
		after	0.54	-	-	0.54

Table 6. Simulated bond length and population of some key bonding involved in adsorption

Bond	Location	Before/after adsorption	Length (Å)	Population
N-H	in amine groups of α-EDA-LA	before	1.031	0.74
		after	1.038	0.35
O---HN	O on quartz surface; H in amine groups of α-EDA-LA	before	3.080	-
		after	1.493	0.04
O-H	on hydroxylated quartz surface	before	0.986	0.53
		after	1.044	0.48

4.2 Collecting mechanism between α-EDA-LA and siderite

4.2.1 Zeta potential of siderite as a function of pH

By comparing Fig. 4 (a) and Fig. 4 (b), it can be found that with the presence of α-EDA-LA, the zeta potential of siderite have been significantly reduced at pH 8.0-10.0. At such pH condition, α-EDA-LA carries negative charges due to the carboxyl group, which exists in the form of $–COO^-$ under alkali condition. As in Fig. 4 (a), the siderite surface is also negatively charged within this pH range. The adsorption of α-EDA-LA on the negatively charged siderite surface caused reductions in the zeta potential. This means the interaction in between overcome the electrostatic repulsion between α-EDA-LA and the siderite surface. The strong interaction enables the excellent collecting ability of α-EDA-LA for siderite at pH 8.0-10.0. This coincides with the flotation results in Fig. 2.

4.2.2 FTIR spectroscopy analysis of siderite

In Fig. 6 (c), the wavenumber region between 1500 cm^{-1} and 400 cm^{-1} contained the infrared spectral features of siderite. The peak at 1416.13 cm^{-1} corresponded to the asymmetrical stretching vibrations of CO_3^{2-}, which is the characteristic peak of siderite. The out-of-plane and in-plane bending vibrations of CO_3^{2-} were defined by the peaks at 868.66 cm^{-1} and 735.94 cm^{-1}, respectively (Peng et al., 1985). The infrared spectral features of α-EDA-LA were observed in the region between 4000 cm^{-1} and 1100 cm^{-1} in Fig. 6 (c). The peaks at 2929.95 cm^{-1} and 2851.15 cm^{-1} proved the adsorption of α-EDA-LA on the surface of siderite, as these peaks were attributed to the stretching vibrations of $–CH_3$ and $–CH_2$- in α-EDA-LA. Hydrogen bond formation between α-EDA-LA and siderite surface was evident from the peak shifts

observed in the comparison of Fig. 6 (a) and Fig. 6 (c). The band centred at 3440.09 cm^{-1} in Fig. 6 (a) shifted 8.29 cm^{-1} to 3431.80 cm^{-1} in Fig. 6 (c). In the lattice structure of siderite, carbon and oxygen atoms inside the geometry of CO_3^{2-} are bonded by covalent bonds. The anions CO_3^{2-} form an anionic field, while the cations Fe^{2+} are scattered in between. CO_3^{2-} and Fe^{2+} are packed closely by ionic bonds. The probability of breaking the covalent bonds inside CO_3^{2-} is much lower than breaking the ionic bonds between CO_3^{2-} and Fe^{2+}. Thus, CO_3^{2-} and Fe^{2+} would be exposed alternately on the surface of siderite upon crushing and grinding. Therefore, the hydrogen bonds between α-EDA-LA and siderite surface were formed by the oxygen atoms on the siderite surface with the electron-deficient hydrogen atoms in the amine groups. The peak, which was originally at 1635.94 cm^{-1} in Fig. 6 (a), experienced a shift of 8.29 cm^{-1} to 1627.65 cm^{-1} in Fig. 6 (c). As discussed previously in section 0, this peak corresponded to the vibration modes of $–NH_2$ and $–COO^-$. The peak shift corroborates the hydrogen bonding between the oxygen atoms exposed on siderite surface and the electron-deficient hydrogen atoms in the amine groups in α-EDA-LA. Additionally, this peak became less obvious after the interaction with siderite. This is due to the coordination of $–COO^-$ and the nitrogen atoms in α-EDA-LA with Fe^{2+} on the siderite surface, which indicates that chemisorption has taken place. Based on the FTIR results, α-EDA-LA was adsorbed on siderite surface dominantly via chemisorption and followed by hydrogen bonding. The schematic diagram of adsorption mechanism is shown in Fig. 8.

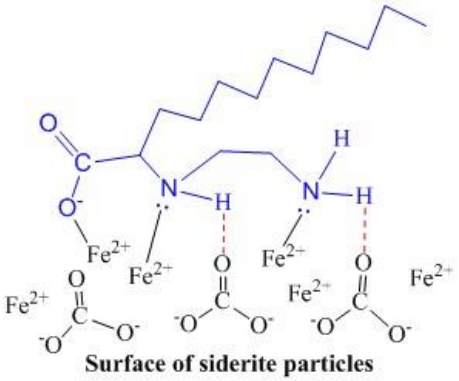

Fig. 8. Schematic diagram: adsorption mechanism of α-EDA-LA on siderite surface (Blue: α-EDA-LA molecule; Black: siderite surface; Solid lines: chemical bonds; Red dashed lines: hydrogen bonds)

4.2.3 Adsorption simulation between α-EDA-LA and siderite

The interaction energy between α-EDA-LA and siderite is calculated as -188.13 kJ/mol. Negative interaction energy reveals the adsorption is spontaneous. The simulation results have proved that the adsorption of α-EDA-LA on siderite surface takes place dominantly via chemisorption. The similarity of O-O distances in minerals and flotation reagents can be used as an indicator of chemical bond formation between O and metal (Gao et al., 2018). The greater the similarity, the stronger the –O-metal and =O metal bonds are. Based on the optimised structures of α-EDA-LA and siderite, the O-O distance in α-EDA-LA is 2.300 Å, presenting a great similarity with O-O distance of 2.269 Å in siderite. Therefore, strong chemical bonds of $–O^-$ Fe^{2+} and =O Fe^{2+} would be formed spontaneously upon adsorption. Electronic analysis was conducted to investigate further the electrons transfer during chemisorption. As presented in Table 7, the population of 2p orbital of O in both C-O and C=O experienced decrease. On the other hand, the population of 4s and 3d orbitals of Fe increased from 0.25 to 0.31 and from 6.63 to 6.72, respectively. This Mulliken population analysis supports that the electrons transferred from O to Fe forming chemical bonds of $–O^-$ Fe^{2+} and =O Fe^{2+}. Furthermore, as per Table 8, a positive population of 0.27 between N atom in α-EDA-LA and Fe^{2+} exposed on siderite surface indicates the chemical bonding of –NH- Fe^{2+} and $–NH_2$- Fe^{2+}. This is further corroborated by the population decrease of N atom in the amine groups of α-EDA-LA as shown in Table 7.

The simulation results in Table 8 show that the N-H bond length in α-EDA-LA increased from 1.031 Å to 1.035 Å, due to the electronic attraction imposed by CO_3^{2-} on siderite. However, the negative populations (-0.06, -0.03 and -0.01) between CO_3^{2-} and H in amine groups of α-EDA-LA indicate that the

electronic attraction did not result in chemical bonds, but intermolecular force, such as hydrogen bonding.

Table 7. Mulliken population analysis of adsorption between α-EDA-LA and siderite surface

Key Atom	Location	Before/after adsorption	s	p	d	Total
O	C-O in α-EDA-LA	before	1.83	4.90	-	6.73
		after	1.84	4.68	-	6.52
O	C=O in α-EDA-LA	before	1.84	4.91	-	6.75
		after	1.82	4.74	-	6.57
Fe	on siderite surface	before	0.25	0.15	6.63	7.03
		after	0.31	0.17	6.72	7.19
N	in α-EDA-LA	before	1.55	4.06	-	5.61
		after	1.58	3.96	-	5.54

Table 8. Simulated bond length and population of some key bonding involved in adsorption

Bond	Location	Before/after adsorption	Length (Å)	Population
N Fe^{2+}	N in α-EDA-LA; Fe^{2+} on siderite surface	after	2.219	0.27
N-H	in amine groups of α-EDA-LA	before	1.031	0.74
		after	1.035	0.73
O---HN	Os in CO_3^{2-} on siderite; H in amine groups of α-EDA-LA	after	-	-0.06/-0.03/-0.01

5. Conclusions

The single mineral and synthetic mixture flotation results showed that, with α-EDA-LA as the collector, quartz could be collected effectively at pH 11.0-12.0 in the reverse flotation. For siderite, the recovery peaked at 83.4% when pH was 8.0, where siderite presented different floatability from magnetite and hematite. Exploiting such difference at pH 8.0 and facilitated by depressants, separation of siderite could be achieved. The zeta-potential studies revealed that the adsorption of α-EDA-LA on the surfaces of siderite and quartz decreased their corresponding zeta potentials at pH of 8.0-10.0 and 8.0-12.0, respectively. This means the adsorptions overcome the electrostatic repulsion between similar charges of α-EDA-LA and the mineral surfaces. The FTIR analyses and molecular simulation suggested that no chemisorption took place between α-EDA-LA and quartz. However, electronic attraction existed between the hydroxylated quartz surface and α-EDA-LA. This electronic attraction could be due to the hydrogen bonding. The adsorption of α-EDA-LA on siderite surface was dominated by the chemisorption, while further enhanced by hydrogen bonding.

Acknowledgement: Great appreciation for the support from National Natural Science Foundation of China (Grant No.: 51274056 and 51474055).

References

AHMED, I., JHUNG, S.H., 2017. *Applications of metal-organic frameworks in adsorption/separation processes via hydrogen bonding interactions*. Chem. Eng. J. 310, 197–215.

CHAIKINA, M.V., KRYUKOVA, G.N., 2004. *Structural transformations in quartz and apatite on mechanical activation*. J. Struct. Chem. 45, 121–126.

CHERNYSHOVA, I.V., RAO, K.H., VIDYADHAR, A., 2000. *Mechanism of adsorption of long-chain alkylamines on silicates: A spectroscopic study. 1. Quartz*. Langmuir 16, 8071–8084.

GAO, Y.S., GAO, Z.Y., SUN, W., HU, Y.H., 2016a. *Selective flotation of scheelite from calcite: A novel reagent scheme*, International Journal of Mineral Processing, 2016, 154,10-15.

GAO, Z.Y., GAO, Y.S., ZHU, Y.Y., HU, Y.H., SUN, W., 2016b. *Selective flotation of calcite from fluorite: a novel reagent schedule*, Minerals, 6 (4), 114.

GAO, Y.S., GAO, Z.Y., SUN, W., YIN, Z.G., WANG, J.J., HU Y.H.,2018. *Adsorption of a novel reagent scheme on scheelite and calcite causing an effective flotation separation.* J. Colloid Interface Sci. 512, 39-46.

GRAF, D.L., 1961. *Crystallographic tables for the rhombohedral carbonates.* Am. Mineral. 46, 1283-1316.

LEVIEN, L., PREVITT, C.T., WEIDNER, D.J., 1980. *Structure and elstic properties of quartz at pressure*. American Mineralogist 65, 920-930.

LI, C., GAO Z., 2017. *Effect of grinding media on the surface property and flotation behavior of scheelite particles*. Powder Technol. 322, 386-392.

LI, L.X., HAO, H.Q., YUAN, Z.T., LIU, J.T., 2017. *Molecular dynamics simulation of siderite – hematite - quartz flotation.* Applied Surface Sci. 419, 557–563.

MOHAMMADNEJAD, S., PROVIS, J.L., VAN DEVENTER, J.S.J., 2013. *Effects of grinding on the preg-robbing potential of quartz in an acidic chloride medium*. Miner. Eng. 52, 31-37.

MULLER-DETHLEFS, K., HOBZA, P., 2000. *Noncovalent interactions: a challenge for experiment and theory*. Chem. Rev. 100, 143–167.

PENG, W.S., LIU, G.K., KE, L.Q., 1985. *Infrared spectra study of magnesite and siderite series*. ACTA Mineralogica Sinica 5, 229-233.

SAHOO, H., RATH, S.S., DAS, B., MISHRA, B.K., 2016. *Flotation of quartz using ionic liquid collectors with different functional groups and varying chain lengths*. Miner. Eng. 95, 107–112.

SCHRAN, C., MARSALEK, O., MARKLAND, T.E., 2017. *Unravelling the influence of quantum proton delocalization on electronic charge transfer through the hydrogen bond.* Chem. Phys. Letters 678, 289-295.

SEO, J., HOFFMANN, W., MALERZ, S., WARNKE, S., BOWERS, M., PAGEL, J., HELDEN, G., 2017. *Side-chain effects on the structures of protonated amino acid dimers: A gas-phase infrared spectroscopy study*. Int. J. Mass Spectrom., http://dx.doi.org/10.1016/j.ijms.2017.06.011

SONG, B.Y., YUAN, L.B., WEI, S.M., 2015. *Investigation on stepped flotation process for carbonate-containing hematite and production practice*. Min. and Metall. Eng. 35, 63-67.

TIAN, M., GAO, Z., HAN, H., SUN, W., HU, Y., 2017. *Improved flotation separation of cassiterite from calcite using a mixture of lead (II) ion / benzohydroxamic acid as collector and carboxymethyl cellulose as depressant*. Miner. Eng. 113, 68-70.

TIAN, Y.A., SUN, B.Q., 2010. *Experimental research on flotation separation of siderite and hematite*. Met. Mine 406, 58-63.

VIDYADHAR, A., RAO, K.H., 2007. *Adsorption mechanism of mixed cationic/anionic collectors in feldspar-quartz flotation system.* J. Colloid Interface Sci. 306, 195–204.

VIDYADHAR, A., RAO, K.H., CHERNYSHOVA, I.V., 2003. *Mechanisms of amine/feldspar interaction in the absence and presence of alcohols studied by spectroscopic methods*. Colloid Surf. A: Physicochem. Eng. Asp. 214, 127–142.

VIDYADHAR, A., RAO, K.H., CHERNYSHOVA, I.V., PRADIP, FORSSBERG, K.S.E., 2002. *Mechanisms of amine–quartz interaction in the absence and presence of alcohols studied by spectroscopic methods*. J. Colloid Interface Sci. 256, 59–72.

VIEIRA, A.M., PERES, A.E.C., 2007. *The effect of amine type, pH, and size range in the flotation of quartz*. Miner. Eng. 20, 1008–1013.

WANG, D.H., LUO, X.M., YIN, W.Z., MA, Y.Q., 2016. *Research on influence of siderite on flotation of hematite and its mechanism*. Non-ferr. Met. – Miner. Process. Section 3, 59-62 & 71.

WENG, S.F., XU, Y.Z., 2016. *Fourier transform infrared spectroscopy*, third ed. Chem. Ind. Press, Beijing.

YANG, B., WU, X.Q., MI, X.X., 2010. *Effect of a-starch in the Separation of Siderite and Hematite*. Min. Metall. Eng. 30, 46-50.

YIN, W.Z., HAN, Y.X., XIE, F., 2010. *Two-step flotation recovery of iron concentrate from Donganshan carbonaceous iron ore*. J. Cent. South Univ. Technol. 17, 750-754.

ZHANG, Z.Y., LV, Z.F., YIN, W.Z., HAN, Y.X., 2008. *Influence of the siderite in Donganshan iron ore on reverse flotation*. Met. Mine 388, 52-55.

ZHU, Y.M., CHEN, J.X., REN, J.L., WANG, T.X., 2014. *Stepped Flotation of Donganshan Mixed Iron Magnetic Concentrate at Normal Temperature Using a New Collector DTX-1.* Met. Mine 457, 61-64.

ZHU, Y.M., LUO, B.B., SUN, C.Y., LIU, J., SUN, H.T., LI, Y.J., HAN, Y.X., 2016. *Density functional theory study of a-Bromolauric acid adsorption on the a-quartz (101) surface.* Miner. Eng. 92, 72-77.